

## RESEARCH ARTICLE

10.1002/2013JB010617

## Key Points:

- A model for boiling two-phase free convective heat transfer is developed
- Heat transfer rates may be further increased by forced convection
- Heat fluxes approach those inferred from observations of some recent eruptions

## Correspondence to:

D. C. Woodcock,  
d.woodcock@lancaster.ac.uk

## Citation:

Woodcock, D. C., S. J. Lane, and J. S. Gilbert (2014), Ice-melt rates in liquid-filled cavities during explosive subglacial eruptions, *J. Geophys. Res. Solid Earth*, 119, 1803–1817, doi:10.1002/2013JB010617.

Received 17 AUG 2013

Accepted 22 FEB 2014

Accepted article online 27 FEB 2014

Published online 24 MAR 2014

## Ice-melt rates in liquid-filled cavities during explosive subglacial eruptions

D. C. Woodcock<sup>1</sup>, S. J. Lane<sup>1</sup>, and J. S. Gilbert<sup>1</sup><sup>1</sup>Lancaster Environment Centre, Lancaster University, Lancaster, UK

**Abstract** Subglacial eruptions are often associated with rapid penetration of overlying ice and release of large flow rates of water as jökulhlaups. Observations of recent subglacial eruptions indicate rapid syn-eruptive ice melting within liquid-filled subglacial cavities, but quantitative descriptions of possible heat transfer processes need to be developed. Calculations of heat flux from the ice cavity fluid to the melting ice surface indicate that up to  $0.6 \text{ MW m}^{-2}$  may be obtained for fluids undergoing single-phase free convection, similar to minimum estimates of heat flux inferred from observations of recent eruptions. Our model of boiling two-phase free convection in subglacial cavities indicates that much greater heat fluxes, in the range  $3\text{--}5 \text{ MW m}^{-2}$ , can be obtained in the vent region of the cavity and may be increased further by momentum transfer from the eruption jet. Rapid magma-water heat transfer from fragmented magma is needed to sustain these heat fluxes. Similar heat fluxes are anticipated for forced convection of subcooled cavity water induced by momentum transfer from an eruption jet. These heat fluxes approach those required to explain jökulhlaup flow rates and rapid ice penetration rates by melting in some, but not all recent eruptions.

### 1. Introduction

Subglacial eruptions melt cavities in the overlying ice, and the resulting meltwater may drain from cavities as it forms or may accumulate within the cavity [Höskuldsson and Sparks, 1997; Gudmundsson, 2003; Gudmundsson et al., 2004; Tuffen, 2007; Magnússon et al., 2012]. Subglacial eruptions where magma has fragmented by granulation or explosion are often characterized by the rapid release of large quantities of water in volcanogenic jökulhlaups, with the subsequent formation of depressions in the surface of the ice sheet or glacier above the site of the eruption. In most cases, the eruption penetrates the overlying ice to become subaerial [Gudmundsson, 2005].

Observations of the effects and duration of subglacial eruptions may provide constraints on ice melting rates and thus on the likely heat transfer processes. Rates of meltwater production during the eruption may be inferred from: (1) the rate of development of depressions in the ice surface above the eruption site, (2) the flow rate of the volcanically induced jökulhlaup or, in some cases, (3) from the flow rate of meltwater into subglacial lakes of known bathymetry [Gudmundsson et al., 2004, 2007; Magnússon et al., 2012]. An additional indication of ice melting rate may be obtained from the rate at which a subglacial eruption penetrates the overlying ice sheet; however, in this case, penetration may be by ice fracturing rather than by wholesale melting. Calorimetry may be applied to inferred ice melting rates to constrain rates of heat transfer during an eruption. These heat transfer rates may then be compared with heat transfer rates calculated for various heat transfer mechanisms.

#### 1.1. Ice Melting Rates and Heat Fluxes in Subglacial Eruptions

Gudmundsson et al. [2004] studied the Gjálp 1996 eruption beneath Vatnajökull, Iceland. Monitoring of the development of ice cauldrons and other depressions in the ice, together with the rise in water level in Grimsvötn, gave two independent measures of meltwater production rate. Around  $3 \text{ km}^3$  of ice was melted during the eruption, with a melting rate of  $0.5 \text{ km}^3$  per day during the first 3 days of the eruption. The heat flux during the first 3 days may be estimated by dividing the power input of 1.8 TW by the heat transfer area. Gudmundsson et al. [2004] used the area of the volcanic edifice as an estimate of the heat transfer area: this was  $3 \text{ km}^2$  for the first 1.5 days, increasing to  $5\text{--}6 \text{ km}^2$ . The resulting heat flux estimate was  $0.5\text{--}0.6 \text{ MW m}^{-2}$  and is likely to be a minimum estimate for the heat flux in the vent region [Gudmundsson et al., 2004].

**Table 1.** Ice Thickness, Duration of Subglacial Phase of the Eruption, Calculated Ice Penetration Rate, and Inferred Melting Heat Flux for Recent Subglacial Explosive Eruptions

| Eruption              | Thickness of Ice (m) | Duration of Subglacial Eruption (h) | Rate of Ice Penetration ( $\text{m h}^{-1}$ ) | Melting Heat Flux ( $\text{MW m}^{-2}$ ) | Reference                  |
|-----------------------|----------------------|-------------------------------------|---|--|----------------------------|
| Gjálp 1996            | 500                  | 30                                  | 17  | 1.4                                      | [Gudmundsson et al., 2004] |
| Eyjafjallajökull 2010 | 200                  | 4                                   | 50  | 4  | [Magnússon et al., 2012]   |
| Deception Island 1969 | 100                  | 2                                   | 50  | 4  | [Smellie, 2002]            |
| Grimsvötn 2004        | 150–200              | 0.5–1                               | 150–400                                       | 12–3                                     | [Jude-Eton et al., 2012]   |
| Katla 1918            | 400                  | 2                                   | 200   | 16                                       | [Gudmundsson, 2005]        |

Table 1 summarizes data for recent subglacial explosive eruptions that penetrated overlying ice. The rate of ice penetration provides an alternative method of calculating the heat flux. Melting heat flux values are calculated assuming that ice penetration is solely by melting.

The ice penetration rates in Table 1 are vertical penetration rates; thus, the corresponding heat fluxes refer to a planar, horizontal ice surface. If the ice surface is sloping at an angle of  $\theta$  to the horizontal, the heat flux required on the surface undergoing melting is reduced by a factor of  $\cos(\theta)$ . In addition, the ice roof may be fractured. Taken together, the effects of surface orientation and fracturing may reduce the required heat flux on the melting surface by a factor of two or more.

We consider the case when syn-eruptive ice melting takes place within ice cavities that are filled with liquid water. Heat transfer from magma to the overlying ice is considered to be a two-stage coupled process in which the convecting cavity fluid acts as an intermediate between the cooling magma and the melting ice. Heat transfer from magma to water has been considered elsewhere [Höskuldsson and Sparks, 1997; Wilson and Head, 2002; Gudmundsson, 2003; Woodcock et al., 2012]. In this paper we examine heat transfer from the cavity liquid water to the overlying roof and walls of the ice cavity, using published heat transfer methods to estimate likely heat fluxes. In particular, we develop a model for boiling two-phase free convection in subglacial cavities. We are not aware of any other study that has taken this approach.

### 1.2. Convective Heat Transfer and Ice Melting in Liquid-Filled Cavities

Figure 1, from Gudmundsson [2003], shows a schematic diagram of an ice cavity formed part way through a fragmentation-dominant subglacial eruption. In the vent region, heat transfer from the hot volcanic particles to the liquid water drives vigorous convection, which in turn causes melting of the overlying ice. The end-

member convection mechanisms are (1) free convection (described as “natural convection” in some references) and (2) forced convection.

Free convection in a liquid water-filled ice cavity is driven by buoyancy forces that are developed by gravity acting on density differences within the water [Turner, 1973]. These density differences may arise by expansion of the water on heating or by local boiling to produce a less dense vapor phase. In the context of a subglacial eruption, forced convection is driven by momentum transfer from the eruption jet of volcanic particles, steam, and other volcanic gases to the surrounding cavity fluid.

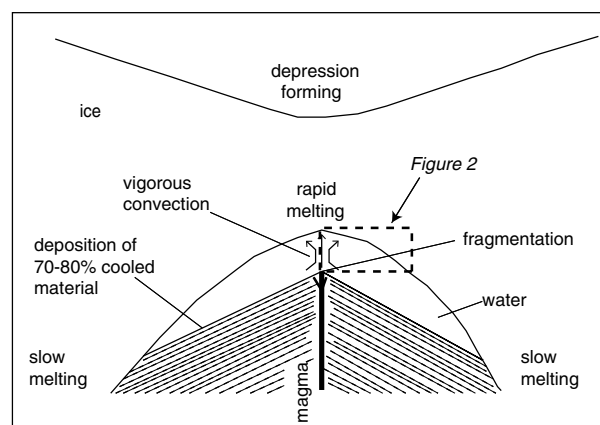


**Figure 1.** Schematic diagram of an ice cavity formed part way through a subglacial eruption where magma is fragmented by granulation or explosion. The dashed rectangle indicates the location of Figure 2. From Gudmundsson, M. T., Melting of ice by magma-ice-water interactions during subglacial eruptions as an indicator of heat transfer in subaqueous eruptions, *Geophysical Monograph*, 140, 61–72, 2003. Copyright [2003] American Geophysical Union. Modified by permission of American Geophysical Union.

## 2. Single-Phase Free Convective Heat Transfer

We consider the case where buoyancy forces are developed by thermal

**Table 2.** Single-Phase Free Convection Heat Transfer Coefficients in a Water-Filled Subglacial Cavity Together With the Corresponding Heat Fluxes

| Bulk Water Temperature | Heat Transfer Coefficient        | Heat Flux          |
|------------------------|----------------------------------|--------------------|
| °C                     | $\text{kW m}^{-2} \text{K}^{-1}$ | $\text{MW m}^{-2}$ |
| 50                     | 0.6                              | 0.03               |
| 100                    | 1.1                              | 0.11               |
| 150                    | 1.6                              | 0.24               |
| 200                    | 2.1                              | 0.42               |
| 250 <sup>a</sup>       | 2.6                              | 0.65               |

<sup>a</sup>Saturation pressure = 4 MPa.

expansion of liquid water, review heat transfer equations for single-phase free convection, and consider the possible complications arising from the 4°C density maximum for water.

The intensity of free convection may be characterized by the Rayleigh number:

$$Ra = \frac{g\alpha\Delta T d^3}{\kappa\nu} \quad (1)$$

where  $g$  is the gravitational acceleration,  $\Delta T$  is the temperature difference,  $d$  is the vertical dimension of the convective motion, and  $\kappa$ ,  $\nu$ , and  $\alpha$  are the thermal diffusivity, kinematic viscosity, and coefficient of thermal expansion, respectively, of the fluid [Turner, 1973].

For Rayleigh numbers appropriate to convection in subglacial cavities, heat transfer in single-phase free convection can be described by:

$$Nu = 0.1Ra^{1/3} \quad (2)$$

where the Nusselt number  $Nu$  is defined as  $Ud/k_l$ , with free convection heat transfer coefficient  $U$  and liquid thermal conductivity  $k_l$  [Huppert and Sparks, 1988; Höskuldsson and Sparks, 1997]. In this case, the free convection heat transfer coefficient is independent of the vertical dimension of the convective motion.

Equation (2) is appropriate for modeling heat transfer by free convection to the horizontal roof of an ice cavity. Heat transfer to the downward-facing sloping walls of the cavity may be modeled by application of results reported by Raithby and Hollands [1998]. For a surface inclined at an angle  $\theta$  to the horizontal, they recommend that the heat transfer coefficient be calculated from:

$$Nu = \max\left[0.13 (Ra \sin\theta)^{1/3}, 0.14 (Ra \cos\theta)^{1/3}\right]. \quad (3)$$

Equation (3) implies that  $Nu$  has a minimum value for a surface sloping at around 45° and that the minimum value is around  $(1/2^{1/2})^{1/3}$  or 90% of the value for a horizontal surface. The effect of surface orientation is thus small and not considered further.

Table 2 gives representative values from equation (2) of heat transfer coefficient for various cavity bulk water temperatures, together with the corresponding heat fluxes. Calculated heat fluxes for cavity water temperatures in excess of 150°C match the heat fluxes calculated in section 1.1 from meltwater production rates but not those inferred from ice penetration rates in Table 1.

The use of the coefficient of thermal expansion in equation (1) implies that the convecting fluid expands uniformly over the whole temperature range of interest. The behavior of water is anomalous: as water is warmed at 0.1 MPa from 0°C, it contracts initially until a maximum density is reached at 4°C [Li et al., 2011]. Thus, in principle, a convecting layer of warm water may be insulated from an overlying ice surface by a convectively stable layer of water. Höskuldsson and Sparks [1997] pointed out this anomalous behavior of water but were concerned with heat removal from magma rather than melting of the overlying ice so did not consider the implications further.

The implications of the 4°C density maximum have attracted considerable attention in the literature. In particular, Tong and Koster [1993] studied numerically a horizontal surface maintained at 0°C. They found that the convective instability in the bulk fluid could penetrate the overlying layer between the density maximum and the cooled surface and erode it completely at higher Rayleigh numbers. As part of a study to investigate possible melting of the roof of a magma chamber, Huppert and Sparks [1988] carried out experiments on the melting of a horizontal “ice roof” by single-phase free convection of warm water, initially at 70°C. They found that their experimental results could be well fitted to a theoretical model that was developed assuming no density maximum. The Rayleigh number of the experiments reported by Huppert and Sparks [1988] was of order  $10^{13}$ , indicating that the warm water was convecting vigorously. The results of Huppert and Sparks [1988] thus seem to corroborate the theoretical study of Tong and Koster [1993]: that the density maximum has a minimal effect on convective heat transfer, provided that convection in the bulk liquid is sufficiently

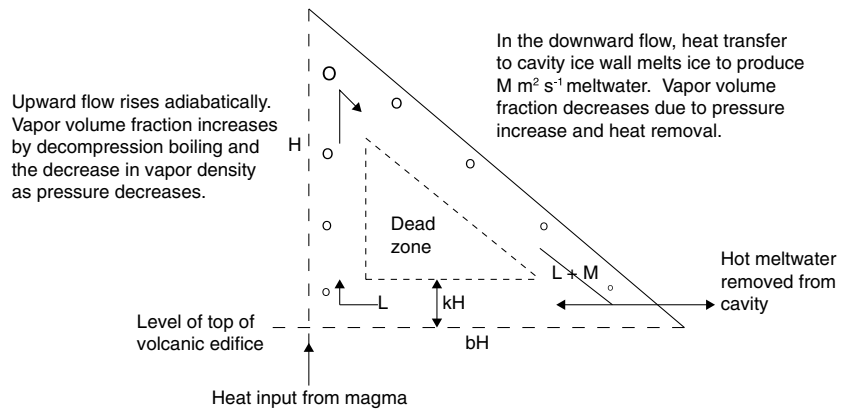


**Figure 2.** Two-phase free convective heat transfer and ice melting in a model subglacial eruption cavity. The cavity is symmetrical about the centerline, and the right-hand half of the cavity only is shown. The third dimension (length) extends into the paper with the model developed for unit length. See Figure 1 for the location within the eruption site.

vigorous. The much greater vertical dimension for convective motion in subglacial cavities will result in Rayleigh numbers well in excess of the value of  $10^{13}$  in the vigorously convecting experiments of *Huppert and Sparks* [1988].

### 3. Two-Phase Free Convective Heat Transfer

#### 3.1. Introduction

Data in Table 2 indicate that a heat flux of  $0.65 \text{ MW m}^{-2}$  at the melting ice surface might be achieved (for a cavity bulk water temperature of  $250^\circ\text{C}$ , the boiling point at 4 MPa). If the heat flux imposed by the subglacial eruption exceeds this value then the water in a cavity with a pressure of 4 MPa will begin to boil. Local boiling above the vent will produce a less dense vapor phase that will induce an enhanced circulation driven by the density difference between the region above the vent and the rest of the cavity.

In this section we explore the resulting two-phase free convection mechanism and attempt to determine likely heat fluxes. In contrast to single-phase free convection, there appears to be no simple equation for heat transfer coefficient in the literature. We have developed a simple model from first principles that captures the essential physics in order to estimate the heat transfer coefficient from the bulk circulation velocity in the cavity. A more detailed model would involve the use of a computational fluid dynamics (CFD) package with multiphase (solid-liquid-vapor) capability [e.g., *Gandhi et al.*, 2011].

#### 3.2. Model Development

Figure 2 shows the elements of the model for the circulation within a prismatic cavity of triangular cross section with a height  $H$  and a basal half width  $bH$ . The triangular shape is chosen for expediency, but the model could be generalized for other geometries. The circulation comprises an upward flow over the vent, followed by a return downward flow along the sloping wall of the cavity (where heat transfer melts ice) followed by a horizontal flow to complete the loop. The flow is assumed to be confined to a channel of width  $kH$  ( $k < 0.5$ ) that is constant for the whole of the circulation. The circulation is thus a “thermosyphon loop” that surrounds a dead zone of stagnant liquid. As a starting point, we assume a constant volume cavity, where melting rates are matched to ductile ice creep rates, together with accumulation rates of erupted material (we discuss how restrictive this assumption is in section 3.5.3). In this case a volume flow  $M$  of meltwater is removed from the cavity, and the return flow  $L$  is recycled to the vent.

The upward flow ascends adiabatically (i.e., approximately at constant enthalpy). Since pressure decreases upward, the local boiling point and thus the liquid enthalpy at the boiling point (the “saturated” enthalpy) will decrease. A vapor phase is present if the flow enthalpy exceeds the saturated liquid enthalpy. The vapor mass fraction increases upward in proportion to the enthalpy excess over saturation. The vapor volume fraction increases upward as both vapor mass fraction and vapor specific volume increase with decreasing pressure.

In the downward flow, vapor volume fraction is decreased as pressure increases (the converse of the upward flow) and, more importantly, by heat transfer from the flow to the cavity ice wall. The average vapor volume fraction in the downward flow is thus less than that in the upward flow; it is this difference that produces the pressure difference that drives the circulation. Circulation is resisted by friction on the cavity ice wall and by energy losses associated with change of direction at the “corners” (Appendix A). The balance of driving force and frictional resistance determines the circulation rate. Heat removed by ice melting and heating of the resulting meltwater is balanced by heat input from the eruption vent.

The principal equations of the model are presented below:

1. Phase equilibrium

For a flow specific enthalpy of  $h$   $\text{kJ kg}^{-1}$ , the vapor mass fraction  $x$  may be calculated from the enthalpy balance:

$$h = xh_g + (1 - x)h_l \quad (4)$$

where  $h_g$  and  $h_l$  are the saturated specific enthalpies of the vapor and liquid respectively.

2. Momentum balance

We assume homogeneous two-phase flow, in which the vapor and liquid velocities are equal (justified in Appendix B). The momentum balance over an element of the flow with height  $dH$ , two-phase density  $\rho$ , velocity  $u$ , and pressure  $P$  is:

$$-dP = \rho g dH + 1/2 \rho_l u_{ls}^2 \Omega_{2\phi} dK + \rho u du \quad (5)$$

where the three terms on the right-hand side are the “gravitational,” “frictional,” and “accelerational” pressure changes, respectively [Whalley, 1987]. The frictional pressure loss is calculated from the liquid density  $\rho_l$ , the superficial liquid velocity  $u_{ls}$ , loss coefficient  $dK$ , and the two-phase multiplier  $\Omega_{2\phi}$  (see Appendix A).

3. Enthalpy balance and heat transfer

Rate of removal of heat  $dQ$   $\text{kJ s}^{-1}$  from a mass flow rate of  $m$   $\text{kg s}^{-1}$  results in a reduction of specific enthalpy  $dh$  of the flow, where:

$$dQ = m dh \quad (6)$$

The upward flow is adiabatic ( $dQ=0$ ). For the downward flow, there is heat transfer from the flow to the ice wall. In this case,

$$dQ = U \Delta T dA \quad (7)$$

where  $dA$  is the heat transfer area,  $\Delta T$  is the temperature difference between the bulk flow and the ice pressure melting point, and  $U$  is the local heat transfer coefficient. The appropriate local heat transfer coefficient is that for turbulent flow parallel to a smooth flat plate. In dimensionless form, the heat transfer coefficient is given by [Incropera and DeWitt, 1996]:

$$Nu_f = 0.0296 Re_f^{0.8} Pr^{1/3} \quad (8)$$

where  $Nu_f$  is the Nusselt number given by  $Uf/k_l$ , where  $f$  is the distance along the surface in the flow direction and  $k_l$  is the liquid thermal conductivity.  $Re_f$  is the Reynolds number given by  $u_l \rho_l f / \mu_l$ , where  $u_l$  is the bulk liquid velocity parallel to the surface and  $\rho_l$  and  $\mu_l$  are the liquid density and viscosity, respectively.  $Pr$  is the Prandtl number given by  $\mu_l C_{pl} / k_l$ , where  $C_{pl}$  is the liquid specific heat capacity.

The calculation procedure used in the model is shown in Figure C1 in Appendix C. Calculations are carried out for each element in turn round the flow loop and the balance between driving and resisting forces checked. If there is an imbalance, the flow rate is adjusted and the calculation sequence repeated.

### 3.3. Results: Reference Case

Figure 3 shows the variation of vapor volume fraction with height within a 50 m high cavity with a basal pressure of 4 MPa (equivalent to an ice thickness of around 400 m above the cavity base). At any height in the cavity the vapor volume fraction in the upward flow exceeds that in the downward flow. The area enclosed by the two curves is proportional to the driving force for the circulation.

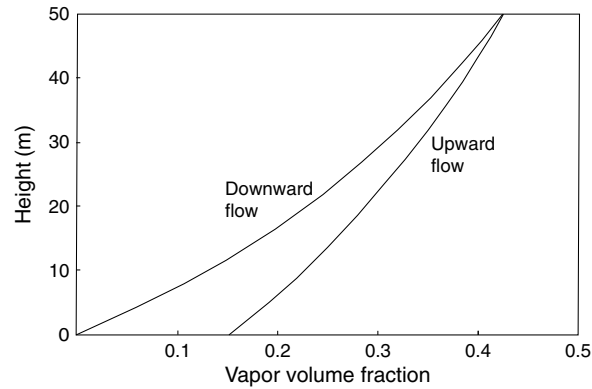


**Figure 3.** Vapor volume fraction within a 50 m high cavity with a basal pressure of 4 MPa. The cavity conditions are those for maximum power in Figure 4 and correspond to the reference case in Table 3.

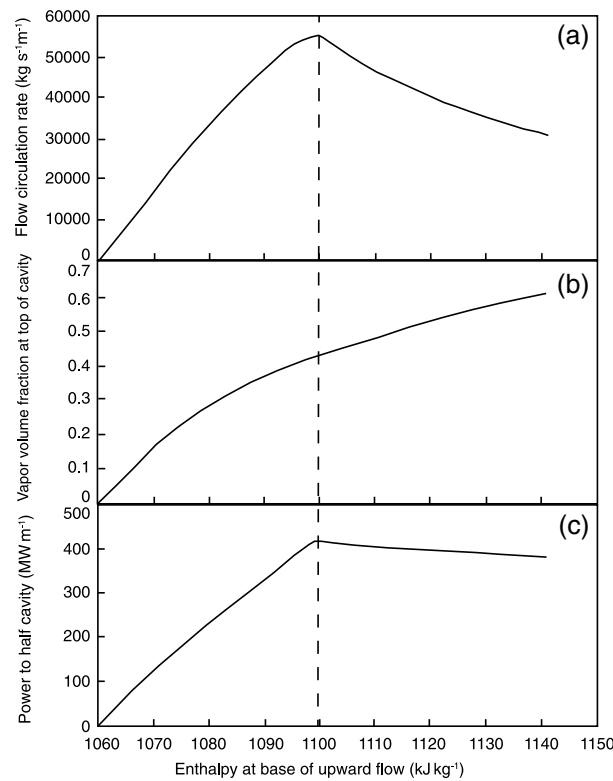


**Figure 4.** Variation of (a) flow circulation rate, (b) vapor volume fraction at the top of the upward flow, and (c) power for two-phase free convection (with no contribution from single-phase convection) within half of a 50 m high cavity at 4 MPa as the enthalpy at the base of the upward flow is varied. Figure 3 and the reference case in Table 3 correspond to maximum power conditions at a fluid enthalpy of 1100 kJ kg<sup>-1</sup>. Figures 4a and 4c show zero circulation rate and power, respectively, at an enthalpy of 1060 kJ kg<sup>-1</sup>, which corresponds to the saturated liquid enthalpy. At this point, single-phase convection would occur as discussed in section 2. Once boiling begins, two-phase convection rapidly overtakes single-phase convection.

Figure 4a shows the variation of flow circulation rate for two-phase free convection within half of a 50 m high cavity at 4 MPa as the enthalpy at the base of the upward flow is varied. Steady-state solutions can only be found over a restricted range of enthalpy (1060 to 1141 kJ kg<sup>-1</sup> in this case). Figure 4b shows the corresponding variation of vapor volume fraction at the top of the upward flow. As the enthalpy is increased from the lowest value, the vapor volume fraction progressively increases, and this drives an increase in circulation rate. A maximum circulation rate is reached at an enthalpy of 1100 kJ kg<sup>-1</sup>. As enthalpy is increased further, the circulation rate decreases, although the vapor volume fraction continues to increase. Thus, over a limited range, the system has two steady states when a given circulation rate may be attained either by relatively low or high vapor volume fractions. Figure 4c shows the corresponding variation of power (for half of the cavity) as the enthalpy at the base of the upward flow is varied. The maximum value at 1100 kJ kg<sup>-1</sup> is a consequence of the velocity-dependent heat transfer coefficient (equation (8)). The proportional reduction in power beyond the maximum is much less than that for the circulation rate, since velocity is determined by vapor volume fraction as well as circulation rate. Figures 4a and 4c show zero circulation rate and power, respectively, at an enthalpy of 1060 kJ kg<sup>-1</sup>, which corresponds to the saturated liquid enthalpy. At this point, single-phase convection would occur as discussed in section 2. Once boiling begins, two-phase convection replaces single-phase convection.

### 3.4. Results: Sensitivity Analysis

Table 3 shows the results from using the model to explore the sensitivity of the system to changes in the input variables (cavity height, cavity aspect ratio, flow area fraction, and the loss coefficient of bends). All cases showed similar behavior to the reference case, in particular, the presence of a maximum power. The results in Table 3 are for the maximum power and for a cavity basal pressure of 4 MPa.

The principal conclusions of the sensitivity study are listed below.

**Table 3.** Sensitivity of Model Results to Changes in Input Variables (Names of Variables Changed Are in Italics) for a Cavity Basal Pressure of 4 MPa

| Variable  | Case      |         |        |        |        |
|---|-----------|---------|--------|--------|--------|
|   | Reference | 2       | 3      | 4      | 5      |
| <i>Cavity height, H (m)</i>   | 50        | 100     | 50     | 50     | 50     |
| <i>Cavity aspect ratio, b</i>                                       | 2         | 2       | 4      | 2      | 2      |
| <i>Flow area fraction, k</i>  | 0.2       | 0.2     | 0.2    | 0.4    | 0.2    |
| <i>Bend loss coefficients, K<sup>a</sup></i>                        | 1         | 1       | 1      | 1      | 0.5    |
| Maximum power <sup>b</sup> (MW m <sup>-1</sup> )                    | 417       | 906     | 1,011  | 315    | 575    |
| Maximum heat flux (MW m <sup>-2</sup> )                             | 3.7       | 4.1     | 4.9    | 2.8    | 5.1    |
| Circulation rate <sup>b</sup> (kg s <sup>-1</sup> m <sup>-1</sup> ) | 55,000    | 123,000 | 74,500 | 78,200 | 82,200 |
| Vapor volume fraction:  |           |         |        |        |        |
| base of upward flow   | 0.153     | 0.153   | 0.229  | 0.100  | 0.136  |
| top of cavity   | 0.428     | 0.557   | 0.463  | 0.407  | 0.424  |
| base of downward flow   | 0.008     | 0.018   | 0.003  | 0.017  | 0.008  |

<sup>a</sup>Factor relative to reference case.

<sup>b</sup>For half of the cavity.

1. Variation in cavity height  $H$  (compare case 2 with reference case)

The area available for flow ( $kH$ ) is proportional to  $H$ , so we might expect circulation rate to be proportional to  $H$ . In fact, circulation rate increases faster than  $H$ , because vapor volume fraction is greater at the top of a higher cavity since pressure is lower. Maximum heat flux on the melting surface increases because the heat transfer coefficient is velocity dependent.

2. Variation in cavity aspect ratio  $b$  (compare case 3 with reference case)

In this case the area available for flow ( $kH$ ) is independent of  $b$ , so the increase in circulation rate with  $b$  is due to the increase in the average vapor volume fraction in the upward flow. Maximum heat flux increases because the heat transfer coefficient is velocity dependent.

3. Variation in flow area fraction  $k$  (compare case 4 with reference case)

The area available for flow ( $kH$ ) is proportional to  $k$ , but the circulation rate is less dependent on  $k$  than expected because vapor volume fraction in the upward flow decreases as  $k$  increases. As a consequence, the reduced heat transfer coefficient causes the maximum heat flux to decrease as  $k$  increases.

4. Variation in bend loss coefficients  $K$  (compare case 5 with reference case)

Circulation rate is almost inversely proportional to  $K^{1/2}$ , as expected for a constant frictional pressure loss. Maximum heat flux shows a slightly weaker dependence in line with the velocity dependence of heat transfer coefficient.

Maximum power (and heat flux) seems to occur when the vapor volume fraction at the base of the downward flow is very low; presumably, this maximizes the vapor volume fraction difference between the upward and downward flows.

Table 4 shows the effect of cavity basal pressure on circulation rate and maximum power, for the reference case cavity dimensions and bend loss coefficients. Maximum power and circulation rate show a weak dependence only on pressure.

Tables 3 and 4 show calculated heat fluxes to the ice melting surface in the range of 3–5 MWm<sup>-2</sup>. These are similar to some of the heat fluxes in Table 1 inferred from ice penetration rates.

### 3.5. Discussion

#### 3.5.1. The Occurrence of a Maximum Heat Flux

The occurrence of a maximum heat flux is not unusual in two-phase natural convection systems. Convective heat transfer within the two-phase boiling “heat pipe” zone in a porous medium above a horizontal heated surface was studied by *Sondergeld and Turcotte* [1977]. The heat pipe zone has a large heat transfer coefficient, with heat conveyed upward in the vapor and the resulting condensate refluxed. Analysis of the heat pipe mechanism shows the presence of a maximum heat flux. *Fukuda and Korobi* [1979] pointed out that two-phase free convection systems are non-linear systems that are prone to complex behavior including multiple steady states.

**Table 4.** The Effect of Cavity Basal Pressure on Circulation Rate and Maximum Power, for the Reference Case Cavity Dimensions ( $H = 50$  m,  $b = 2$ ,  $k = 0.2$ )

| Variable   | Cavity Basal Pressure (MPa) |        |        |        |
|--|-----------------------------|--------|--------|--------|
|  | 6                           | 4      | 2      | 1      |
| Cavity top pressure (MPa)  | 5.7                         | 3.7    | 1.8    | 0.84   |
| Maximum power <sup>a</sup> ( $\text{MW m}^{-1}$ )                  | 397                         | 417    | 435    | 436    |
| Maximum heat flux ( $\text{MW m}^{-2}$ )                           | 3.6                         | 3.7    | 3.9    | 3.9    |
| Circulation rate <sup>a</sup> ( $\text{kg s}^{-1} \text{m}^{-1}$ ) | 50,000                      | 55,000 | 55,600 | 45,300 |
| Vapor volume fraction:   |                             |        |        |        |
| base of upward flow  | 0.111                       | 0.153  | 0.253  | 0      |
| top of cavity  | 0.300                       | 0.428  | 0.653  | 0.812  |
| base of downward flow  | 0                           | 0.008  | 0.016  | 0      |

<sup>a</sup>For half of the cavity.

### 3.5.2. Critical (Choked) Flow

In a channel of a constant cross-sectional area, the flow velocity cannot exceed the speed of sound. In two-phase (vapor-liquid) mixtures the speed of sound is much reduced compared with that of the single-phase liquid and vapor end-members because the two-phase mixture has a gas-like bulk modulus but a liquid-like density [Kieffer, 1977]. For homogeneous two-phase flow, calculation of the speed of sound depends on the degree to which equilibrium is maintained between the vapor and liquid phases during the passage of a sound wave [Kieffer, 1977; Whalley, 1987]. There are two limiting cases to be considered: (1) homogeneous frozen flow, when the vapor mass fraction remains constant and phase equilibrium is not maintained, and (2) homogeneous equilibrium flow, where the vapor mass fraction adjusts to maintain phase equilibrium. Kieffer [1977] graphically summarizes the results of calculations for liquid water-steam mixtures for both limiting cases; these show that the speed of sound is reduced if phase equilibrium is maintained. Whalley [1987] presents an equivalent graph for homogeneous equilibrium flow.

Table 5 shows the critical circulation rates for the four cavity pressures studied in section 3.4, together with the corresponding circulation rates from Table 4. In all the cases studied the circulation rate was below the critical circulation rate.

### 3.5.3. Steady-State Versus Growing Cavity

Our model assumes a steady-state situation with a cavity of constant size from which meltwater is removed at cavity temperature. This is a convenient form of model because it allows the overall heat balance to be checked for accuracy. A constant size cavity requires that melt-back is balanced by ductile creep and the accumulation of erupted material; this is unlikely to be the case in general. However, for the 4 MPa reference case, the circulation time of the liquid is around 25 s for a cavity with a height of 50 m. The melt-back rate is  $3 \text{ mm s}^{-1}$ , equivalent to 0.075 m during one liquid circulation time. We assume that the equilibrium circulation is established quickly, say within five liquid circulation times, during which the melt-back is 0.37 m or 0.7% of the cavity height.

## 4. Forced Convective Heat Transfer

### 4.1. Introduction

This section considers forced convection in which an external source of energy such as a jet of high-speed fluid transfers momentum to the surrounding fluid by entrainment. It builds on the suggestion in Höskuldsson and Sparks [1997] that natural circulation may be enhanced by “mechanical stirring” of the water-filled cavity

**Table 5.** Critical Circulation Flow Rates Compared With Circulation Flows Calculated for Cases at Maximum Power

|   | Cavity Basal Pressure (MPa) |         |         |        |
|---|-----------------------------|---------|---------|--------|
|   | 6                           | 4       | 2       | 1      |
| Critical circulation rate <sup>a</sup> ( $\text{kg m}^{-1} \text{s}^{-1}$ ) | 260,000                     | 200,000 | 130,000 | 70,000 |
| Maximum circulation rate ( $\text{kg m}^{-1} \text{s}^{-1}$ )               | 50,000                      | 55,000  | 55,600  | 45,300 |

<sup>a</sup>Calculated from Whalley [1987].

by the explosive eruption. We restrict consideration to a preliminary assessment of convection forced by eruption jets together with a brief review of ice drilling with hot water.

#### 4.2. Convection Forced by Eruption Jets

An explosive eruption emerges from a vent opening into a liquid-filled cavity as a jet with mainly upward momentum. The jet comprises a mixture of volcanic particles, steam, and other volcanic gases (of varying solubility in water). We discuss the effect of each component on the fluid flow and heat transfer processes involved. In general, the circulation induced by momentum transfer will be modified by free convection due to density differences between the jet and the surrounding water.

Volcanic particles will impart momentum to the cavity water as the jet entrains fluid; however, the particles will be denser than the fluid, so will increase the average density of the jet and thus reduce the buoyancy effect. Particles will be hot on ejection, and the smaller diameter particles will cool significantly during the time taken for the jet to mix. Heat loss will be by a combination of intraparticle conduction and surface boiling [Woodcock *et al.*, 2012] to generate additional steam within the jet. This steam will provide additional buoyancy but not momentum. During the early stages of cavity formation, volcanic particles may be carried up to the cavity roof with sufficient momentum to mechanically abrade the ice surface. In addition, the presence of the particles enhances heat transfer coefficients by disturbing the boundary layer between the bulk fluid and the ice surface [Ozbelge, 2001].

Steam, both magmatic and produced by phreatomagmatism, is expected to be a major component of the erupting jet. Steam will “drive” the circulation of cavity fluid by momentum transfer and positive buoyancy. If the cavity water is subcooled, the steam will progressively condense.

The other volcanic gases will also drive circulation by momentum transfer and buoyancy. The main volcanic gas (after water) is likely to be CO<sub>2</sub>. The extent of dissolution of CO<sub>2</sub> in the cavity water will be determined by the partial pressure of CO<sub>2</sub> in the gas phase once any steam has condensed and by the temperature of the cavity water. Any undissolved gas will tend to accumulate within the cavity unless vented.

Head and Wilson [2003] examined the entrainment of sea water into a magmatically produced jet of eruption products. They consider the entrainment zone as a Prandtl jet within which the eruption jet mixes with the surrounding cold seawater in a predictable geometric pattern. Mixing is considered to be complete when the jet has risen a height of c. 6 times the width  $W$  of the vent. At this point, the jet has a width of c. 2.5  $W$ . If the vent width is similar to a typical dyke width of 1 m [Gudmundsson *et al.*, 2004], the entrainment zone would be 6 m high and up to 2–3 m wide. The vent width is poorly constrained but is likely to be considerably larger than the width of the feeding dyke.

Head and Wilson [2003] carried out a momentum balance to determine the final velocity of the jet when entrainment is complete. They assume that all the magmatic steam condenses and all magmatic CO<sub>2</sub> dissolves (and justify these assumptions for the entrainment of cold seawater). Thus, they do not consider any buoyancy driving force from the jet. It may be necessary to modify their analysis if the cavity water is too hot to satisfy their assumptions.

For illustrative purposes, we consider a wholly magmatic explosive eruption of a basaltic magma containing 1 wt.% water. We assume a cavity with a water pressure of 2 MPa and a cavity water temperature sufficiently cool to satisfy the assumptions in Head and Wilson [2003]. Application of the equations in Head and Wilson [2003] gives a velocity of c. 30 m s<sup>-1</sup> once entrainment is complete. The resulting axial zone of water and particles will continue to decelerate and broaden as it moves upward toward the ice cavity roof. If unconstrained, it would rise an additional 45 m before coming to rest. Within the confines of an ice cavity, the flow pattern will be considerably more complicated. A full treatment of forced convective heat transfer and ice melting in subglacial eruption cavities probably needs to be approached by computational fluid dynamics modeling.

#### 4.3. Ice Drilling With Hot Water

Holes in ice sheets and glaciers are drilled using jets of hot water to induce intense forced convective heat transfer at the base of the hole. The British Antarctic Survey (BAS) developed a hot water drilling system using water at 80°C that was able to drill shallow holes at 100 m h<sup>-1</sup> and to attain depths of 560 m [Makinson, 1993].

More recent developments by BAS [Makinson, 2003] envisaged drilling holes at  $40 \text{ m h}^{-1}$  to depths of 2000 m using hot water at  $90^\circ\text{C}$ .

Ice drilling rates are comparable with an ice penetration rate of  $17 \text{ m h}^{-1}$  inferred for the Gjalp subglacial eruption. However, these drilling rates are achieved by forced convection of hot water from a nozzle that is optimally placed with respect to the ice melting surface. Hot water drilling rates thus probably indicate an upper bound of what might be achieved in a liquid-filled subglacial cavity. The morphology of a developing subglacial cavity will be determined by melting, provided that external factors such as ice flow predominantly from one direction do not interfere greatly. The cavity roof may not be optimally placed relative to the vent; separations greater than optimum will incur additional entrainment of cavity liquid, thus reducing both velocity and temperature at the stagnation point on the cavity roof. However water temperatures may be well in excess of  $80\text{--}90^\circ\text{C}$ ; other things being equal, this will increase the temperature driving force for forced convective heat transfer.

Martin *et al.* [2006] presented the results of a modeling study of hot water drilling that was developed to optimize drilling performance in the multi-hole drilling program in connection with the IceCube neutrino observatory at the South Pole. This project involved the drilling of 0.5 m diameter holes to a depth of 1300 m in ice at  $-40^\circ\text{C}$ . Drilling rates of  $70 \text{ m h}^{-1}$  were achieved using hot water at  $90^\circ\text{C}$  ( $70^\circ\text{C}$  at the nozzle at maximum depth). A CFD model is used to calculate the flow velocity field around the base of the borehole. Local heat transfer coefficients are then calculated from local water velocity and temperature. Martin *et al.* [2006] showed wide variations in heat transfer coefficient between the center and the periphery of the hole, thus demonstrating that simple models based on an average heat transfer coefficient are unlikely to be useful.

## 5. Discussion

We have considered free and forced convective heat transfer within liquid-filled subglacial cavities during explosive eruptions in order to make estimates of heat fluxes on the ice melting surfaces. We review these estimates and the implications for ice melting during subglacial eruptions.

### 5.1. A Possible Complication: The Accumulation of Insoluble Gases

Insoluble magmatic gases, together with air released from the ice on melting, are likely to accumulate at the top of the ice cavity. Höskuldsson and Sparks [1997] observed that melting rates for the roof were much less than those for the walls in their laboratory scale ice cavity and considered this to be due to air accumulation at the top of the cavity. The heat fluxes calculated above do not include any allowance for accumulation of insoluble gases. The effect might be to progressively blind the heat transfer area at the apex of the cavity and thus to reduce the total area available for heat transfer on the ice cavity wall.

A possible way of removing insoluble gases from the cavity might be by venting them to the surface up a crevasse in the ice. Gudmundsson *et al.* [2004] noticed the presence of an echelon fractures on the ice surface above the Gjalp 1996 eruption site on aerial photographs taken on 1 October, before the eruption became subaerial. They suggest that the fractures may be the surface expression of a basal crevasse that was produced by tensional stresses associated with dyke intrusion at the start of the subglacial eruption and that fractures might be of the order of 1 m wide. If a fracture in the ice exists from cavity to surface, then insoluble gases may vent from the top of the cavity up through the water column in the fracture.

### 5.2. The Implications for Ice Melting During Subglacial Eruptions

Heat fluxes calculated for single-phase free convection of cavity water can match minimum values inferred for subglacial eruptions (section 1.1). Much larger heat fluxes (Figure 5) can be obtained by two-phase free convection within a cavity with water at its boiling point, at least in the region of the vent.

Höskuldsson and Sparks [1997] calculated that the conductive heat flux from a basaltic effusive eruption could generate vigorous single-phase free convection with cavity water temperatures of up to  $100^\circ\text{C}$ . Magma fragmentation by granulation or explosion is thus required to provide the power input needed to drive two-phase free convection. We anticipate that momentum transfer from an eruption jet will enhance the circulation, resulting in heat fluxes to the ice surface that match the melting rates inferred for the Gjalp 1996 eruption.

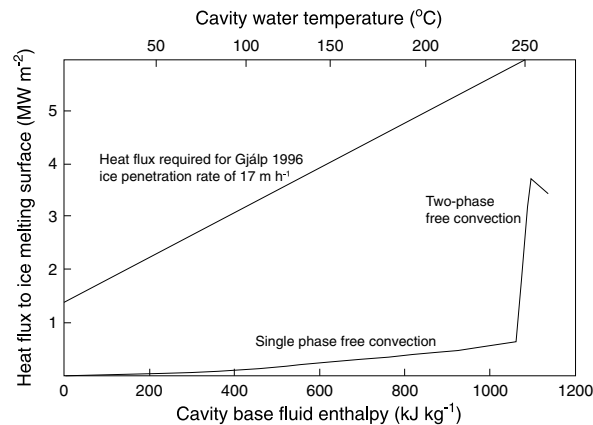


**Figure 5.** Heat flux to the ice melting surface for both single-phase and two-phase free convection as a function of cavity basal fluid enthalpy, together with the heat flux required to match the Gjalp 1996 ice penetration rate by melting and heating the resulting melt-water to cavity temperature. The cavity water temperatures corresponding to the enthalpy values are shown on the upper horizontal axis. Data are for a 50 m high cavity with a basal pressure of 4 MPa (boiling point 250°C). Single-phase free convection heat fluxes are from Table 2; two-phase free convection heat fluxes are for the reference case in Table 3.

Ice penetration rates achieved during ice drilling suggest an alternative scenario that may achieve the melting rates inferred for the Gjalp 1996 eruption. This comprises a cavity that contains hot but subcooled water in which circulation is forced by momentum transfer from a particularly vigorous eruption jet.

Our calculations suggest that penetration rates of around 10–20 m h<sup>-1</sup> might be attained by two-phase free convection or forced convection; however, penetration rates of 200 m h<sup>-1</sup>, as demonstrated by the 1918 Katla eruption, imply heat fluxes of around 16 MW m<sup>-2</sup>. These heat fluxes appear to be well in excess of values likely to be achievable by convective heat transfer alone in liquid-filled cavities.

Our two-phase free convection model indicates maximum power in the range of 500–1000 MW per m length of erupting fissure. This is equivalent to the production of 1500–3000 m<sup>3</sup> s<sup>-1</sup> of meltwater at 0°C per km. The average flow rate of water from the Gjalp 1996 eruption into Grimsvötn was

6000 m<sup>3</sup> s<sup>-1</sup> for the first 3 days of the eruption, when the fissure length was 2–3 km [Gudmundsson *et al.*, 2004]. We conclude that two-phase convection, as envisaged in our model, can explain the heat transfer rates needed to produce the jökulhlaup flows observed in recent eruptions.

## 6. Conclusions

We have used published heat transfer computation methods to make preliminary estimates of heat fluxes on the ice melting surfaces within liquid-filled subglacial cavities during explosive eruptions. For two-phase free convection, we have developed a model to estimate the circulation velocity within the cavity. The principal conclusions are as follows:

1. Heat fluxes of up to 0.6 MW m<sup>-2</sup> can be obtained by single-phase free convection in liquid-filled cavities. These heat fluxes are similar to minimum estimates of heat flux inferred from observations of recent eruptions.
2. Heat fluxes calculated from observations of ice penetration rates are in the range from 1.4 MW m<sup>-2</sup> to around 20–30 MW m<sup>-2</sup>.
3. Heat fluxes of 3–5 MW m<sup>-2</sup> can be attained by two-phase free convection in liquid-filled cavities. These approach the heat fluxes required to match the inferred ice melting rates for the Gjalp 1996 eruption. Eruptions in which magma is fragmented by granulation or explosion are needed to provide the two-phase free convection heat fluxes, and explosive eruptions may enhance convection by momentum transfer from the eruption jet.
4. Hot water ice drilling rates suggest that similar heat fluxes may be attained by convection of subcooled cavity water forced by an eruption jet.
5. The extreme rates of ice penetration observed at some eruptions suggest that convective heat transfer within liquid-filled cavities needs to be supplemented by additional mechanisms.
6. The jökulhlaup flows observed in recent eruptions may be adequately explained by syn-eruptive ice melting.

## Notation

- A* area for heat transfer, m<sup>2</sup>
- b* ratio of cavity half width to height, dimensionless

|                     |   |
|---------------------|---|
| $C_f$               | friction factor, dimensionless  |
| $C_{pl}$            | liquid specific heat capacity, $\text{J kg}^{-1} \text{K}^{-1}$                 |
| $d$                 | vertical dimension for convection, m  |
| $f$                 | distance in flow direction, m   |
| $g$                 | acceleration due to gravity, $\text{m s}^{-2}$                                  |
| $H$                 | cavity height, m  |
| $h$                 | flow specific enthalpy, $\text{kJ kg}^{-1}$                                     |
| $h_g$               | saturated vapor specific enthalpy, $\text{kJ kg}^{-1}$                          |
| $h_l$               | saturated liquid specific enthalpy, $\text{kJ kg}^{-1}$                         |
| $K$                 | loss coefficient for a bend, dimensionless                                      |
| $k$                 | ratio of channel width to cavity height, dimensionless                          |
| $k_l$               | liquid thermal conductivity, $\text{W m}^{-1} \text{K}^{-1}$                    |
| $L$                 | liquid circulation flow rate per unit cavity length, $\text{m}^2 \text{s}^{-1}$ |
| $M$                 | meltwater flow rate per unit cavity length, $\text{m}^2 \text{s}^{-1}$          |
| $m$                 | mass flow rate, $\text{kg s}^{-1}$  |
| $Nu$                | Nusselt number, dimensionless   |
| $P$                 | pressure, Pa  |
| $Pr$                | Prandtl number, dimensionless   |
| $Q$                 | heat transfer rate, $\text{J s}^{-1}$   |
| $Ra$                | Rayleigh number, dimensionless  |
| $Re$                | Reynolds number, dimensionless  |
| $U$                 | heat transfer coefficient, $\text{W m}^{-2} \text{K}^{-1}$                      |
| $u$                 | two-phase fluid velocity, $\text{m s}^{-1}$                                     |
| $u_l$               | bulk liquid velocity, $\text{m s}^{-1}$   |
| $u_{ls}$            | superficial liquid velocity, $\text{m s}^{-1}$                                  |
| $u_s$               | slip velocity, $\text{m s}^{-1}$  |
| $u_t$               | terminal velocity, $\text{m s}^{-1}$  |
| $x$                 | vapor mass fraction, dimensionless  |
| $W$                 | width of vent, m  |
| $\Delta T$          | temperature difference, K   |
| $\alpha$            | coefficient of thermal expansion, $\text{K}^{-1}$                               |
| $\kappa$            | thermal diffusivity, $\text{m}^2 \text{s}^{-1}$                                 |
| $\mu_l$             | liquid dynamic viscosity, Pa s  |
| $\nu$               | kinematic viscosity, $\text{m}^2 \text{s}^{-1}$                                 |
| $\varphi$           | vapor volume fraction, dimensionless  |
| $\rho$              | two-phase fluid density, $\text{kg m}^{-3}$                                     |
| $\rho_g$            | vapor density, $\text{kg m}^{-3}$   |
| $\rho_l$            | liquid density, $\text{kg m}^{-3}$  |
| $\tau$              | shear stress, Pa  |
| $\theta$            | angle of inclination of surface to horizontal, degree                           |
| $\Omega_{2\varphi}$ | two-phase multiplier, dimensionless   |

## Appendix A: Frictional Pressure Losses

### A1. Energy Loss at Bends

Figure 2 shows that the circulation path contains a right angle bend and two acute angle bends. Flow around a bend in pipes and open channels results in an energy loss from flow separation and secondary flow. Both mechanisms are consequences of the radial pressure gradient and dissipate energy in the flowing system by transferring momentum across the flow [Massey, 1970; Francis, 1969]. This loss may be represented conventionally by a pressure loss  $\Delta P_{bend} = K \rho_l u_l^2 / 2$ , where  $K$  is the loss coefficient for the bend. Table A1 gives loss coefficients for bends in pipe systems for various values of the ratio of bend radius to pipe diameter.

**Table A1.** Loss Coefficients for 90° Circular Bends [Tilton, 2007]

|                           | Bend Radius/Pipe Diameter |      |     |     |
|---------------------------|---------------------------|------|-----|-----|
|                           | 1                         | 2    | 3   | 5   |
| Loss coefficient <i>K</i> | 0.35                      | 0.25 | 0.2 | 0.2 |

The circulation path in the ice cavity model comprises flow in a long channel between a stagnant core and the ice wall or base rather than in a pipe. A secondary circulation cannot develop in this case, but flow separation will occur in a bend wherever the flow is in contact with the ice cavity wall. The use of loss

coefficients based on pipe flow is thus likely to overestimate the energy losses in the bends within the ice cavity circulation.

For the non-circular flow cross section, we use the concept of hydraulic diameter to replace the pipe diameter in Table A1. In the ice cavity circulation path in Figure 2, the hydraulic diameter is  $2kH$ , with  $k=0.2$  in the reference case used.

The right angle bend has a bend radius of around  $H$ ; the appropriate value of  $K$  is thus around 0.25. For the other two bends, Tilton [2007] suggested increasing the values obtained from Table A1 by a factor of 1.2 to allow for the more acute angle. The bend radius for these two bends is around  $0.5H$ ; the appropriate value of  $K$  for this bend type is thus around 0.4. These values are likely to overestimate the losses within the ice cavity. The sensitivity of circulation rate to the values of loss coefficients chosen is explored in section 3.4.

The discussion above establishes provisional values for loss coefficients based on single-phase flow. For homogeneous two-phase flow, the single-phase loss coefficients are increased by a “two-phase multiplier”  $\Omega_{2\phi}$ :

$$\Omega_{2\phi} = x \frac{\rho_l}{\rho_g} + (1 - x) \quad (A1)$$

where  $\rho_l$  and  $\rho_g$  are the saturated liquid and vapor densities, respectively, and  $x$  is the vapor mass fraction [Whalley, 1987].

### A2. Wall Frictional Pressure Drop

For an element of the downward flow along the cavity ice wall, the wall frictional pressure drop  $dP_{wf}$  may be determined from a force balance:

$$\tau(1 + b^2)^{1/2} dH = kHdP_{wf} \quad (A2)$$

where  $\tau$  is the shear stress on the surface, which is conventionally expressed as  $\tau = C_f * \frac{1}{2} \rho_l u_l^2$  where  $C_f$  is the friction factor and  $u_l$  is the liquid velocity.

We assume that the ice cavity wall is smooth, so that the friction factor  $C_f$  may be expressed as:

$$C_f = 0.074Re^{-0.2} \quad (A3)$$

where  $Re$  is the Reynolds number of the liquid flow [Incropera and DeWitt, 1996].

In practice, values of  $C_f$  are such that the resistance to circulation is dominated by pressure loss due to the bends.

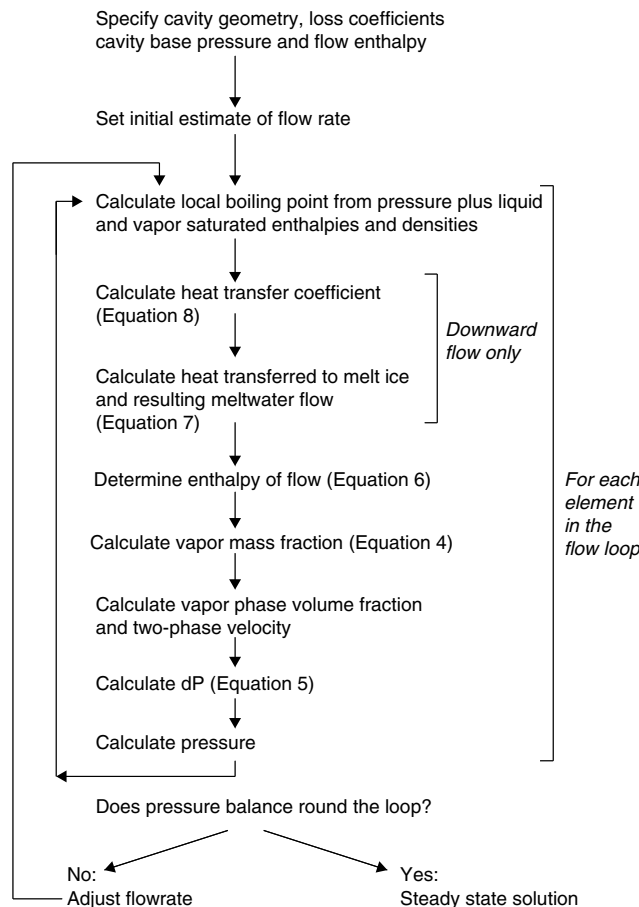


**Figure C1.** Calculation procedure used in the model developed for two-phase free convective heat transfer in an ice cavity.

## Appendix B: Slip Velocity

The slip velocity  $u_s$  (the velocity of the vapor phase relative to the liquid phase) can be related to the terminal rise velocity of a bubble  $u_t$  by equation (B1):

$$u_s = u_t(1 - \phi)^n \quad (\text{B1})$$

where  $\phi$  is the vapor volume fraction ("voidage" or "void fraction" in the engineering literature) and the exponent  $n$  has a value of around 2 [Kay and Nedderman, 1985].

Clift *et al.* [1978] indicate that the maximum stable air bubble size in water at S.T.P. is c. 50 mm. The corresponding rise velocity is  $0.5 \text{ m s}^{-1}$ . The maximum stable size of a bubble of steam in water at elevated temperatures remains to be determined. A bubble is destabilized by a decrease in surface tension, and the rate of development of instability increases as viscosity decreases [Clift *et al.*, 1978]; thus, maximum bubble size should decrease as temperature increases.

The model results in section 3.3 show that liquid velocities are typically  $5\text{--}10 \text{ m s}^{-1}$  at high power and that vapor volume fractions are typically up to 0.5. Slip velocity is thus likely to be less than 10% of liquid velocity. For this preliminary model, we have assumed zero slip velocity. The effect of neglecting slip velocity will be to slightly increase the vapor volume fraction in the upward flow and to decrease it slightly in the downward flow. The net effect will be to slightly increase the circulation driving force and thus the power at steady state.

## Appendix C: Calculation Procedure for Two-Phase Free Convective Heat Transfer Model

Figure C1 shows the calculation procedure used in the model developed in section 3 for two-phase free convective heat transfer in an ice cavity.

### Acknowledgments

We sincerely thank Magnus Tumi Gudmundsson for his detailed comments during review which have greatly improved the paper. We also thank an anonymous reviewer, the Editor André Revil, and the Associate Editor for their comments. We are grateful to Lionel Wilson for comments on an early version of this paper.

### References

- Clift, R., J. R. Grace, and M. E. Weber (1978), *Bubbles, Drops and Particles*, Dover, New York.
- Francis, J. R. D. (1969), *A Textbook of Fluid Mechanics*, Edward Arnold, London, U. K.
- Fukuda, K., and T. Korobi (1979), Classification of two-phase flow instability by density wave oscillation model, *J. Nucl. Sci. Technol.*, *16*, 95–108.
- Gandhi, M. S., M. J. Sathe, J. B. Joshi, and P. K. Vijayan (2011), Two-phase natural convection: CFD simulations and PIV measurement, *Chem. Eng. Sci.*, *66*, 3152–3171.
- Gudmundsson, M. T. (2003), Melting of ice by magma-ice-water interactions during subglacial eruptions as an indicator of heat transfer in subaqueous eruptions, in *Explosive Subaqueous Volcanism*, Geophys. Monogr. Ser., vol. 140, edited by J. D. L. White, J. L. Smellie, and D. A. Clague, pp. 61–72, AGU, Washington, D. C., doi:10.1029/140GM04.
- Gudmundsson, M. T. (2005), Subglacial volcanic activity in Iceland, in *Iceland: Modern Processes, Past Environments, Developments in Quaternary Science*, vol. 5, edited by C. J. Caseldine *et al.*, pp. 127–151, Elsevier, Amsterdam, Netherlands.
- Gudmundsson, M. T., F. Sigmundsson, H. Bjornsson, and T. Hognadottir (2004), The 1996 eruption at Gjalp, Vatnajökull ice cap, Iceland: Efficiency of heat transfer, ice deformation and subglacial water pressure, *Bull. Volcanol.*, *66*, 46–65.
- Gudmundsson, M. T., T. Hognadottir, A. B. Kristinsson, and S. Gudbjornsson (2007), Geothermal activity in the subglacial Katla caldera, 1999–2005, studied with radar altimetry, *Ann. Glaciol.*, *45*, 66–77.
- Head, J. W., and L. Wilson (2003), Deep submarine pyroclastic eruptions: theory and predicted landforms and deposits, *J. Volcanol. Geotherm. Res.*, *121*, 155–193.
- Höskuldsson, A., and R. S. J. Sparks (1997), Thermodynamics and fluid dynamics of effusive subglacial eruptions, *Bull. Volcanol.*, *59*, 219–230.
- Huppert, H. E., and R. S. J. Sparks (1988), Melting the roof of a magma chamber containing a hot, turbulently convecting fluid, *J. Fluid Mech.*, *188*, 107–131.
- Incropera, F. P., and D. P. DeWitt (1996), *Introduction to Heat Transfer*, John Wiley & Sons, New York.
- Jude-Eton, T. C., T. Thordarson, M. T. Gudmundsson, and B. Oddsson (2012), Dynamics, stratigraphy and proximal dispersal of supraglacial tephra during the ice-confined 2004 eruption at Grimsvötn Volcano, Iceland, *Bull. Volcanol.*, *74*, 1057–1082.
- Kay, J. M., and R. M. Nedderman (1985), *Fluid Mechanics and Transfer Processes*, Cambridge Univ. Press, Cambridge, U. K.
- Kieffer, S. W. (1977), Sound speed in liquid-gas mixtures: Water-air and water-steam, *J. Geophys. Res.*, *82*, 2895–2904.
- Li, Y.-R., X.-F. Yuan, C.-M. Wu, and Y.-P. Hu (2011), Natural convection of water near its density maximum between horizontal cylinders, *Int. J. Heat Mass Transfer*, *54*, 2550–2559.
- Magnússon, E., M. T. Gudmundsson, G. Sigurdsson, M. J. Roberts, F. Höskuldsson, and B. Oddsson (2012), Ice-volcano interactions during the 2010 Eyjafjallajökull eruption, as revealed by airborne radar, *J. Geophys. Res.*, *117*, B07405, doi:10.1029/2012JB009250.
- Makinson, K. (1993), The BAS hot water drill: Development and current design, *Cold Reg. Sci. Technol.*, *22*, 121–132.
- Makinson, K. (2003), Future hot water drilling on Rutford Ice Stream 2004/5, *FRISP Report*, *14*, 167–172.
- Martin, R. A., T. Thompson, N. Ansari, and C. Guetari (2006), IceCube CFD drilling model, *Proceedings of FEDSM2006: 2006 ASME Joint U.S.-European Fluids Engineering Summer Meeting*, pp. 157–170.
- Massey, B. S. (1970), *Mechanics of Fluids*, Van Nostrand Reinhold, London, U. K.
- Ozbelge, T. A. (2001), Heat transfer enhancement in turbulent upward flows of liquid–solid suspensions through vertical annuli, *Int. J. Heat Mass Transfer*, *44*, 3373–3379.
- Raithby, G. D., and K. G. T. Hollands (1998), Natural convection, in *Handbook of Heat Transfer*, 3rd ed., edited by W. M. Rohsenow, J. P. Hartnett, and Y. I. Cho, pp. 4.1–4.99, McGraw Hill, New York.

- Smellie, J. L. (2002), The 1969 subglacial eruption on Deception Island (Antarctica): Events and processes during an eruption beneath a thin glacier and implications for volcanic hazards, *Geol. Soc. Spec. Publ.*, *202*, 59–79.
- Sondergeld, C. H., and D. L. Turcotte (1977), An experimental study of two-phase convection in a porous medium with applications to geological problems, *J. Geophys. Res.*, *82*, 2045–2053.
- Tilton, J. N. (2007), Fluid and particle dynamics, in *Perry's Chemical Engineers' Handbook*, 8th ed., edited by D. W. Green and R. H. Perry, pp. 6.4–6.54, McGraw Hill, New York.
- Tong, W., and J. N. Koster (1993), Penetrative convection of sublayer of water including density inversion, *Heat Mass Transfer*, *29*, 37–49.
- Tuffen, H. (2007), Models of ice melting and edifice growth at the onset of subglacial basaltic eruptions, *J. Geophys. Res.*, *112*, B03203, doi:10.1029/2006JB004523.
- Turner, J. S. (1973), *Buoyancy Effects in Fluids*, Cambridge Univ. Press, Cambridge, U. K.
- Whalley, P. B. (1987), *Boiling, Condensation, and Gas-Liquid Flow*, Clarendon Press, Oxford, U. K.
- Wilson, L., and J. W. Head (2002), Heat transfer and melting in subglacial basaltic volcanic eruptions: implications for volcanic deposit morphology and meltwater volumes, *Geol. Soc. Spec. Publ.*, *202*, 5–26.
- Woodcock, D. C., J. S. Gilbert, and S. J. Lane (2012), Particle-water heat transfer during explosive volcanic eruptions, *J. Geophys. Res.*, *117*, B10205, doi:10.1029/2012JB009240.